Hydrodynamic Analysis Inside a Circulating Fluidized Bed Boiler Based on Time Change Using CFD

Tony Suryo Utomo[1,*], Eflita Yohana[1], Rayhan Halim[1], Mohammad Farkhan Hekmatyar Dwinanda[2], Zakaria Rahmanu[1], Kwang-Hwan Choi[3]

[1] Department of Mechanical Engineering, Diponegoro University, Jl. Prof. Sudharto, SH., Semarang 50275, Indonesia
[2] Dept Energy Conservation & Loss Control, Engineering Development, Ref Unit V Balikpapan, PT Kilang Pertamina International, Indonesia
[3] College of Engineering, Pukyong National University, 365 Sinseon-ro, Nam-gu, Busan 608-739, Republic of Korea

ARTICLE INFO	ABSTRACT
          	The power generation industry has progressively improved the design of power plants to tackle global climate change. Coal-fired power plants will be cleaner and more efficient with the CFB (Circulating Fluidized Bed) technology in the boiler. CFB boilers have the advantage where the resulting carbon dioxide, SOx, and NOx emissions are significantly reduced. This makes research on CFB boilers widely carried out, especially those using CFD (Computational Fluid Dynamic). This study aims to determine the most appropriate turbulence model using CFD simulations on CFB boilers to analyze the hydrodynamic elements in the boiler against time changes, including the distribution of solid volume fractions, pressure, velocity, and wall shear stress. Three turbulence models were tested as part of the simulation: standard $k-\varepsilon$, RNG $k-\varepsilon$, and RSM, which were then compared to earlier research. The RNG $k-\varepsilon$ model produces the closest result to the experimental data, with an error value of 6.24%. Solid volume fraction area is increasingly widespread with values ranging from 0.05 to 0.1 from the furnace's bottom to a height of 15 m. The high-pressure area further expands at the bottom of the furnace to a height of 15 m, with values ranging from 3 kPa to 10 kPa. The outlet line velocity has increased from 43 m/s to 50 m/s. The wall shear stress increases from 0.75 Pa to 1.1 Pa at the outlet wall.

1. Introduction

Currently, the world is experiencing global climate change, which impacts natural disasters. This has become the most pressing environmental problem facing humanity [1,2]. The United Nations Framework Convention on Climate Change states that Indonesia is committed to contributing to global climate change solutions. One of the solutions is to reduce greenhouse gas (GHG) emissions, which cause global warming. This is caused by deforestation and forest fires, as well as emissions from the power generation sector's usage of fossil fuels (petroleum and coal) [3], requiring emission management to be considered, followed by suitable mitigation measures [4]. Therefore, the power

---

generation industry has progressively improved the design of power plants to meet increasingly stringent air pollution limits.

Boiler are the main component in the power generation system. One of the types is the coal-fired boiler. Currently, coal dominates the fuel mix due to its availability and lower cost compared to other hydrocarbon fuels [5]. Of several types of boilers, CFB boilers have more efficient combustion with cleaner exhaust gases than other types of boilers [6]. CFB Boiler has an advantage resulting in significantly reduced carbon dioxide, SOx, and NOx emissions, making the emissions cleaner and friendly to the environment [7-10]. The emissions can be reduced without complicated burners or extra exhaust gas treatment facilities [11]. Compared to pulverized coal (PC) boilers, it requires a longer ignition time and has unstable combustion at low loads [12]. The combustion/gasification of high alkaline coal in CFB boilers is more beneficial [13]. The furnace temperature in a CFB boiler (approximately 800-900°C) is lower than a PC boiler (approximately 1300-1700°C). As a result, less liquid ash particles will be produced and the release of sodium from coal particles would be prevented. So further research is needed to understand CFB boilers to be appropriately utilized [9].

In theoretical and practical investigations, the complexity of the hydrodynamic patterns and behavior of CFB boiler combustion is sometimes a challenge due to the paucity of study on this subject [14]. Technological developments encourage researchers to use computational fluid dynamics (CFD) simulations. This is because CFD can provide a cost-effective way of understanding fluid flow characteristics to simulate the processes of CFB boilers. This makes the design and operation can be optimized [15,16].

In general, CFB Boiler model consists of a gas-solid multiphase flow structure where two materials are used: air material and bed material. Bed material or solid material functioned as a sorbent that absorbs emissions and excess heat [17]. CFB Boiler research using CFD simulations has now been widely carried out [18,19]. There are different turbulence model used by several previous researchers, including standard $k - \varepsilon$ model and RNG $k - \varepsilon$ model [20]. Amoo used standard $k - \varepsilon$ model in the CFB boiler simulation, which explains that the error value from the simulation results validated that carried out on experimental data is 10% based on the temperature value in the furnace [21]. RNG $k - \varepsilon$ model is used in the CFB boiler simulation by Ji *et al.,* which explains that the error value of the simulation results validation carried out on the experimental data is 8.9% based on the value of the NO gas concentration in the furnace [13].

Therefore, it is necessary to research the comparison of the two turbulence models and other turbulence models, specifically to RSM, which in theory can provide more accurate results in CFD simulations on CFB Boilers. This study aims to determine the turbulence model in the CFD simulation on the CFB Boiler to see which model is the most appropriate to use. In addition, hydrodynamic analysis was carried out on changes in time which included the distribution of solid volume fractions, pressure, velocity, and wall shear stress.

2. Methodology
2.1 Builder Equation
2.1.1 Mass conservation

The Eulerian multiphase granular flow model is used to visualize the fluidized bed flow, which is composed of two phases that are a fluid phase and a solid phase. The continuity equation or mass conservation in the Eulerian multiphase model for the solid phase, which is solved by ANSYS Fluent can be written in Eq. (1) [22].

$$\frac{\partial}{\partial t}(\alpha_q \rho_q) + \nabla \cdot (\alpha_q \rho_q \vec{v}_q) = \sum_{p=1}^{n}(\dot{m}_{pq} - \dot{m}_{qp}) + S_q \tag{1}$$

2.1.2 Momentum conservation

Multi-fluid granular model was used in ANSYS Fluent to explain the flow of fluid-solid mixtures. The solid phase stress is calculated by coupling the thermal motion of the gas intake molecules with the inelastic granular phase and the random motion of the particles resulting from particle collisions. The momentum conservation equation for the solid phase in the Eulerian multiphase model can be calculated through Eq. (2) [22].

$$\frac{\partial}{\partial t}(\alpha_q \rho_q \vec{v}_q) + \nabla \cdot (\alpha_q \rho_q \vec{v}_q \vec{v}_q)$$
$$= -\alpha_q \nabla p + \nabla \cdot \bar{\bar{\tau}}_q + \alpha_q \rho_q \vec{g} + \sum_{p=1}^{n}(\vec{R}_{pq} + \dot{m}_{pq} \vec{v}_{pq} - \dot{m}_{qp} \vec{v}_{qp})$$
$$+ (\vec{F}_q + \vec{F}_{lift,q} + \vec{F}_{wl,q} + \vec{F}_{vm,q} + \vec{F}_{td,q}) \tag{2}$$

2.1.3 Turbulence model

Three methods for modeling turbulence in multiphase flow on the $k - \varepsilon$ are offered by ANSYS Fluent. In addition, ANSYS Fluent provides two turbulence options in the Reynolds Stress Model (RSM) [22].

The $k - \varepsilon$ turbulence model has several options, including example

  i.   mixed turbulence
  ii.   dispersed turbulence model
  iii. each phase's turbulence model

The RSM turbulence model has several options, including
Options for the RSM turbulence model include:

  i.   dispersed turbulence model
  ii.   mixed turbulence model

The standard $k - \varepsilon$ turbulence model is based on the model transport equation for the kinetic energy (k) and its dissipation rate (ε). For fully turbulence flow, where the influence of molecular viscosity in its derivatives is insignificant, the standard $k - \varepsilon$ model is utilized. Eq. (3) and Eq. (4) are used to calculate the kinetic energy (k) and dissipation rate (ε) of turbulence [22,23].

$$\frac{\partial}{\partial t}(\rho k) + \frac{\partial}{\partial xi}(\rho k u_i) = \frac{\partial}{\partial xj}\left[\left(\mu + \frac{\mu t}{\sigma k}\right)\frac{\partial k}{\partial x_j}\right] + Gk + Gb - \rho\varepsilon - Y_M + Sk \tag{3}$$

$$\frac{\partial}{\partial t}(\rho\varepsilon) + \frac{\partial}{\partial xi}(\rho\varepsilon u_i) = \frac{\partial}{\partial xj}\left[\left(\mu + \frac{\mu t}{\sigma\varepsilon}\right)\frac{\partial\varepsilon}{\partial x_j}\right] + C_{1\varepsilon}(Gk + C_{3\varepsilon} + Gb) - C_{2\varepsilon}\rho\frac{\varepsilon^2}{k} - Y_M + S\varepsilon \tag{4}$$

Advantages of the RNG k-ε models compared to Standard k-ε models include [22]

i. The RNG model adds extra terms in the ε equation that improve the accuracy for fast strain flow in the equation.
ii. RNG model enhances rotational flow accuracy by taking into account the vortex effect on turbulence.
iii. For turbulent Prandtl numbers, the RNG theory gives an analytical equation, whereas the standard $k - \varepsilon$ model employs a user-defined constant value.
iv. For high Reynolds number models, such as the standard $k - \varepsilon$ are used. Additionally, the RNG model offers a viscous flow analytical calculation solution that consider a low Reynolds number.

RNG $k - \varepsilon$ model form is written in Eq. (5) and Eq. (6) [22].

$$\frac{\partial}{\partial t}(\rho k) + \frac{\partial}{\partial xi}(\rho k u_i) = \frac{\partial}{\partial xj}\left[\alpha_k \mu_{eff}\frac{\partial k}{\partial x_j}\right] + Gk + Gb - \rho\varepsilon - Y_M + Sk \tag{5}$$

$$\frac{\partial}{\partial t}(\rho\varepsilon) + \frac{\partial}{\partial xi}(\rho\varepsilon u_i) = \frac{\partial}{\partial xj}\left[\alpha_k \mu_{eff}\frac{\partial\varepsilon}{\partial x_j}\right] + C_{1\varepsilon}\frac{\varepsilon}{k}(Gk + C_{3\varepsilon}Gb) - C_{2\varepsilon}\rho\frac{\varepsilon^2}{k} - R\varepsilon + S\varepsilon \tag{6}$$

In order to account for the effect of streamlined curvature, rotation, eddies, and rapid changes in strain rate, the Reynolds Stress Model (RSM) is more rigorous than the one-equation and two-equation. This shows that RSM is very capable of providing accurate predictions for complicated flows. The RSM is applied when the flow characteristic is caused by anisotropy in the Reynolds voltage. Examples are cyclone flow, high vortex flow in the combustion chamber, rotating flow line, and voltage-induced secondary flow in the line. The transport equation for RSM can be written in Eq. (7) [22].

$$\begin{aligned}
\frac{\partial}{\partial t}\left(\rho u'_i u'_j\right) &+ \frac{\partial}{\partial x_k}\left(\rho u_k u'_i u'_j\right) \\
&= -\frac{\partial}{\partial x_k}\left[\rho u'_i u'_j u'_k + p'\left(\delta_{kj}u'_i + \delta_{ik}u'_j\right)\right] + \frac{\partial}{\partial x_k}\left[\mu\frac{\partial}{\partial x_k}\left(u'_i u'_j\right)\right] \\
&- \rho\left(u'_i u'_k\frac{\partial u_j}{\partial x_k} + u'_j u'_k\frac{\partial u_i}{\partial x_k}\right) - \rho\beta\left(g_i u'_j\theta + g_j u'_i\theta\right) + p'\left(\frac{\partial u'_i}{\partial x_j} + \frac{\partial u'_j}{\partial x_i}\right) \\
&- 2\mu\frac{\partial u'_i}{\partial x_k}\frac{\partial u'_j}{\partial x_k} - 2\rho\Omega_k\left(u'_j u'_m \varepsilon_{ikm} + u'_i u'_m \varepsilon_{jkm}\right) + S_{user}
\end{aligned} \tag{7}$$

2.2 Research Objects

This research was conducted based on the simulations conducted previously by Zhang *et al.,* The CFB boiler in this study located in Guangdong, China and was created by Harbin Boiler Co. Ltd. [24]. In the CFB boiler, two types of working phases are the gas phase in the form of air material and the solid phase in the form of bed material. In the form of sand, bed material serves as a sorbent that absorbs SO_2 pollutants and excess heat. This drives the combustion process to produce a lower temperature. The combustion temperature produced by the CFB boiler is 800-900°C, while the combustion temperature produced by the PC boiler is 1300-1700°C. Therefore, the decreasing

temperature in the CFB boiler will reduce the formation of NOx. This sorbent differentiates between CFB-type boilers and other boilers [7]. The simulation method used is according to the simulation in Zhang *et al.,* [24]. The hydrodynamic CFD simulation on the CFB boiler aims to determine the most appropriate turbulence model and analyze the distribution of solid volume fractions, pressure, velocity, and wall shear stress. The results observed in this simulation were taken at time intervals of 10, 20, 30, and 40 seconds. The boiler reaches a steady state at 40 seconds [24].

2.3 Geometry and Mesh

The geometry design was made based on the CFB boiler design, as stated in the research of Zhang *et al.,* [24]. The design shown in Figure 1 consists of 2 cyclones made to collect sorbent particles and unburned fuel to be returned to the furnace, which is the combustion chamber [25]. The furnace has dimensions of 15.32 × 36.5 × 7.22 m, and each cyclone has a diameter of 8.08 m.
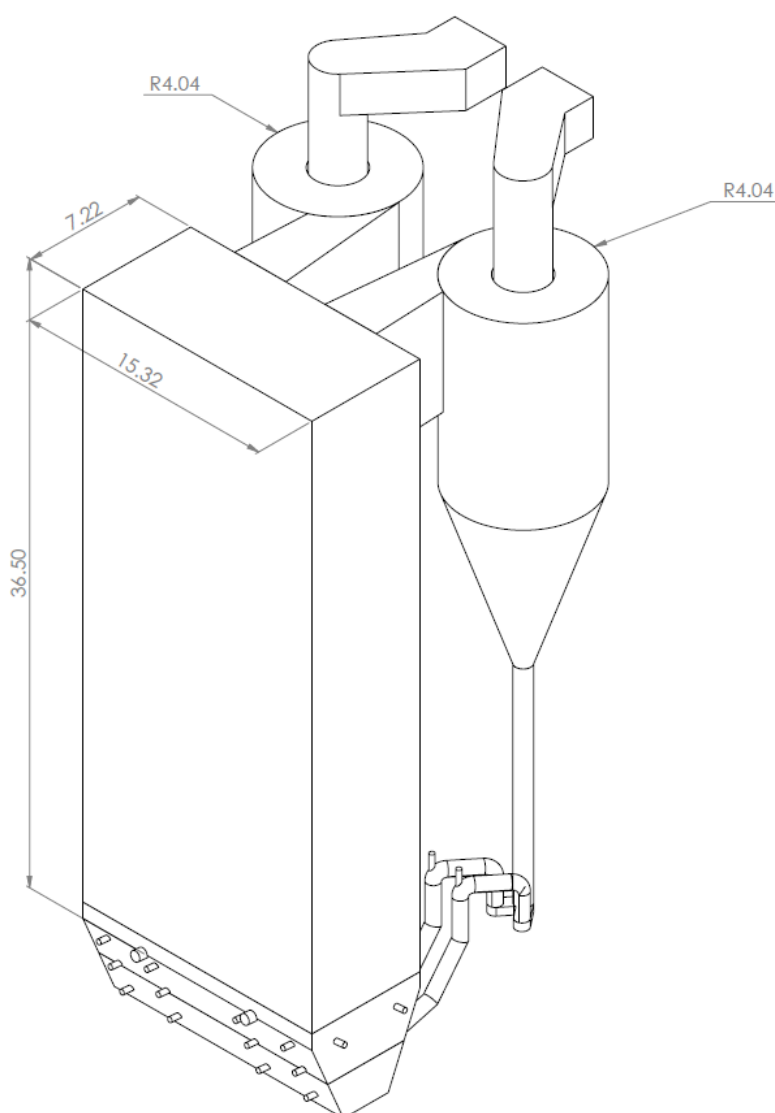
Fig. 1. Boiler geometry design [24]

The meshing used is according to the simulation method of Zhang *et al.,* [24], which are polygonal and hexahedral types shown in Figure 2. In making a polygonal mesh, the first step is creating a tetrahedral mesh in ANSYS Meshing and then converting it into a polygonal mesh in ANSYS Fluent

[26]. The allowable skewness value is below 0.75. This number is included in the appropriate category shown in Table 1 [27].
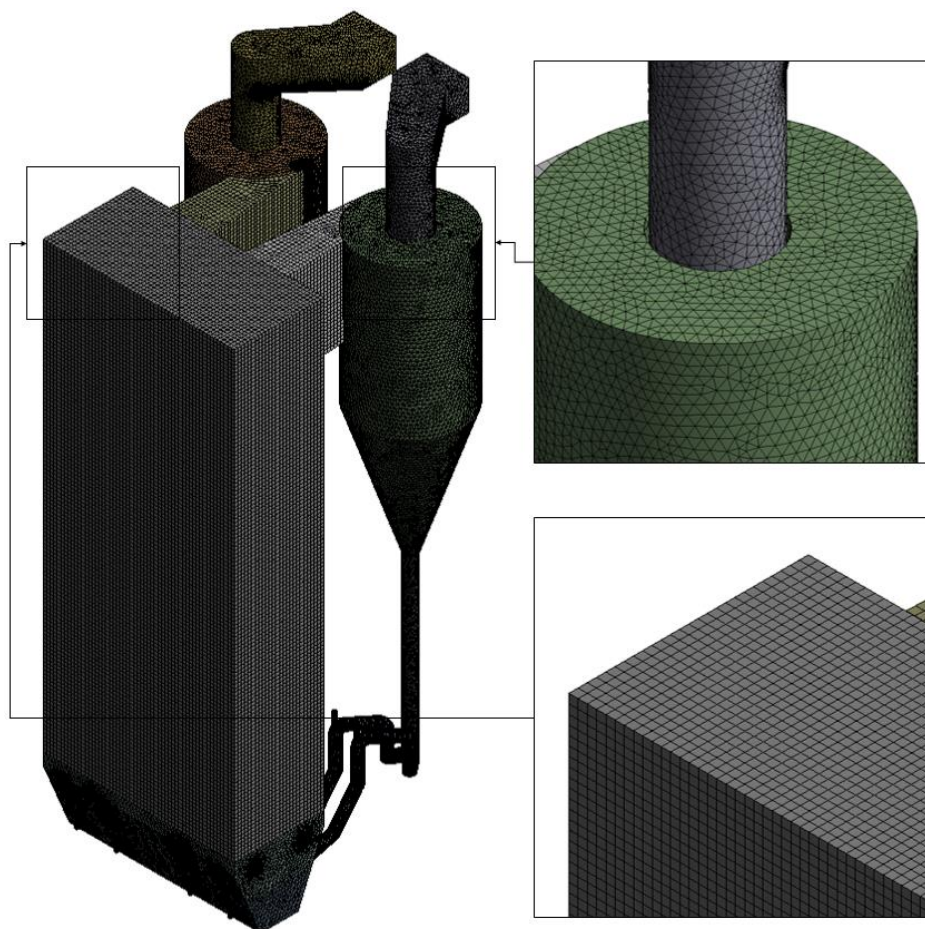
Fig. 2. Meshing on boiler [24]

Table 1
Meshing quality value in Ansys [27]

Value of Skewness	Quality of Cell
0	equilateral
>0 to 0.25	excellent
0.25 to 0.5	good
0.5 to 0.75	fair
0.75 to 0.9	poor
0.9 to <1	bad (silver)
1	degenerate

2.4 Simulation Settings

The simulation modeling in this study is shown in Table 2. The multiphase model uses Eulerian because this model is used for two separate phases, but both can interact. The Viscous models tested were standard $k - \varepsilon$, RNG $k - \varepsilon$, and RSM. The option of the multiphase turbulence model used a dispersed turbulence model because the model is specialized for granular flow [22].

Table 2
Circulating Fluidized Bed boiler simulation model [22,24]

Type	Information	Election Basis
Multiphase	Eulerian	Used for modeling separate phases, but interacting with each other
Viscous	Standard k-ε	the flow is assumed to be fully turbulent
	RNG k-ε	enhancing accuracy for swirling flows
	RSM	enhancing accuracy for swirling flows
Turbulence multiphase model	Dispersed	Used when the model is granular flow

The value of material properties is shown in Table 3. The density values of gas and solid materials and the viscosity of gaseous materials are taken from the research of Zhang *et al.,* [24]. The viscosity value of solid material follows the gas material [26].

Table 3
Material properties [24, 26]

Properties	Material	
	Gas	Solid
Density (kg/^{m3})	0.2928	2000
Viscosity (kg/ms)	$4.71×10^{-5}$	$4.71×10^{-5}$

Table 4 contains specific information regarding the properties of the granular phase materials. A two-phase flow model with granular kinetic flow theory was used to predict hydrodynamic phenomena [28].

Table 4
Granular properties [24]

Properties	Settings
Diameter	0.0002 m
Frictional viscosity	Schaeffer
Granular temperature	Phase property
Granular bulk viscosity	Lun *et al.,*
Granular viscosity	Gidaspow

The value of boundary condition is adjusted to the simulation data of Zhang *et al.,* in order to obtain accurate value that are close to the experimental data [24]. The boundary conditions are shown in Table 5. Figure 3 show the boundary condition areas, which consist of (1) primary air inlet, (2) secondary air inlet, (3) slag-cooler inlet, (4) loop-seal inlet, (5) coal-feed inlet, and (6) cyclone outlet [24].

Table 5
Boundary conditions [24]

Boundary conditions	Mass flow rate (kg/s)	
	Fluid phase	Solid phase
Primary air inlet	94.16	0
Secondary air inlet	53.2	0
Slag-cooler inlet	8	0
Loop-seal inlet	2.32	0
Coal-feed inlet	12.48	0
Boundary conditions	Fluid phase	Solid phase
Cyclone outlet	pressure outlet (default)	
Wall	no slip	partial slip (0.6)
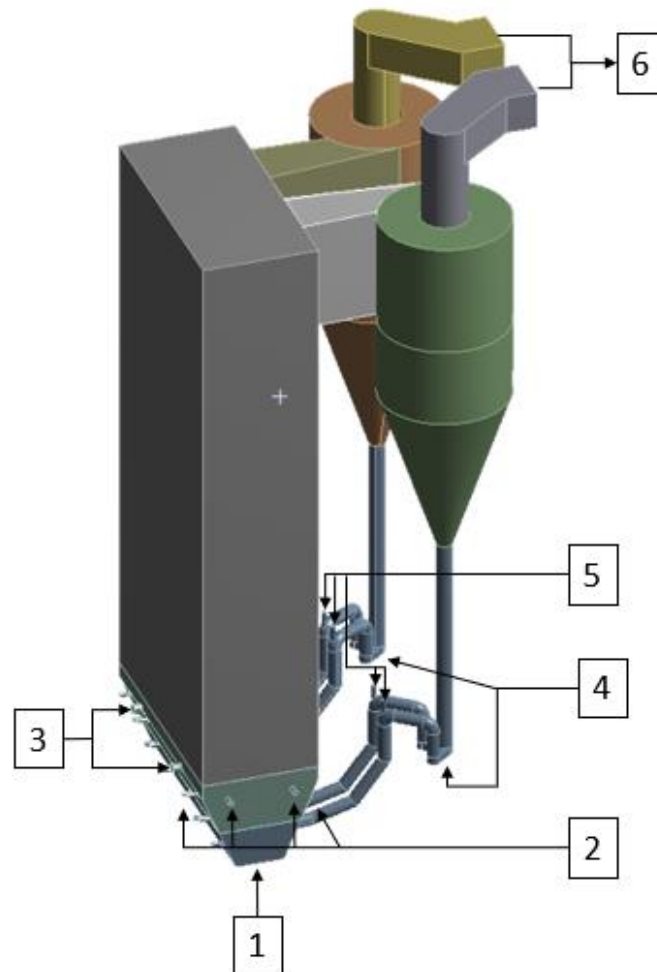
Fig. 3. Boundary conditions

2.5 Solution

Hybrid initialization is used in this simulation. The concrete pile with a value of solid volume fraction of 0.4 is initially inserted in the furnace at a height of 0 to 2.5 m. The height value is inputted in the region adaptation menu, and then the patch menu is selected to enter the solid volume fraction value [26]. SIMPLE method is used for pressure-velocity coupling, while first-order upwind solves the spatial discretization of momentum and volume fraction [24]. The simulation ran in 40 seconds with a time step size of 0.5 seconds.

2.6 Independent Grid Test

The independent grid test in this study aims to select the correct number of cells so that the simulation results are obtained accurately. Meshing is done by testing five variations in the number of cells that is 517000, 548000, 593000, 649000, and 741000. Figure 4 shows the velocity at both outlets, which became stable, around 39 m/s in the simulation using a cell number of 649000, with error values for the highest number of cells at 1.08% and 1.23% at both outlets. This value is already below the allowable error value of 10% [21,29]. Therefore, the simulation with the number of cells 649000 will be used in this research.
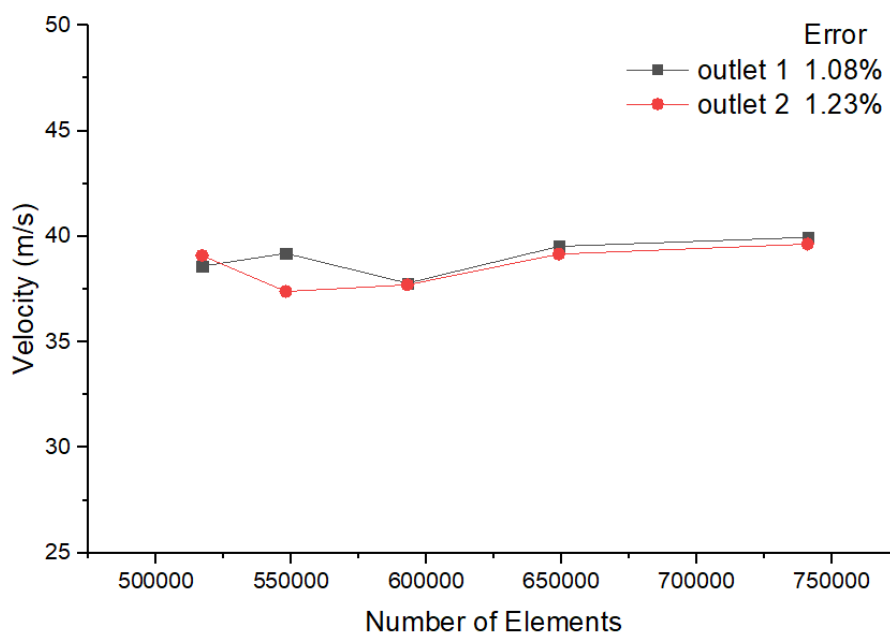
Fig. 4. Velocity graph on both outlets with 5 variations in cell count

3. Results
3.1 Validation of Results

The research by Zhang *et al.,* compared the simulation result with experimental and simulation data. This is done to ensure that the results of the simulation method used are valid and select a turbulence model whose results are closest to the experimental data. Thus, the model can be selected for use in further CFB Boiler research. The validation process is carried out by comparing the pressure drop value in the furnace from a height of 0 - 30 m. Figure 5 illustrates the comparison of the pressure distribution values between the simulation results and three turbulence models as well as experiments and simulations by Zhang *et al.,* The error value obtained from the pressure drop is 6.59% with the standard $k - \varepsilon$ model, 6.24% with the RNG $k - \varepsilon$ model, and 6.36% with the RSM, indicating that the maximum permitted error limit of 10% has been met [28]. In addition, the error values from the simulations of Zhang *et al.,* to the experimental data is 8.55% by the RNG $k - \varepsilon$ turbulence model, which makes this model have the most minor error value in this study. Figure 6 also shows that the simulation with the RNG $k - \varepsilon$ model produces a higher pressure inside the furnace at the height of 15 - 30 m compared to the standard $k - \varepsilon$ model and RSM, which makes the value is closer to the experimental data. Therefore, it can be said that the RNG $k - \varepsilon$ is the most appropriate model to be used in the CFD simulation on the CFB boiler because the results are closest to the experimental data.
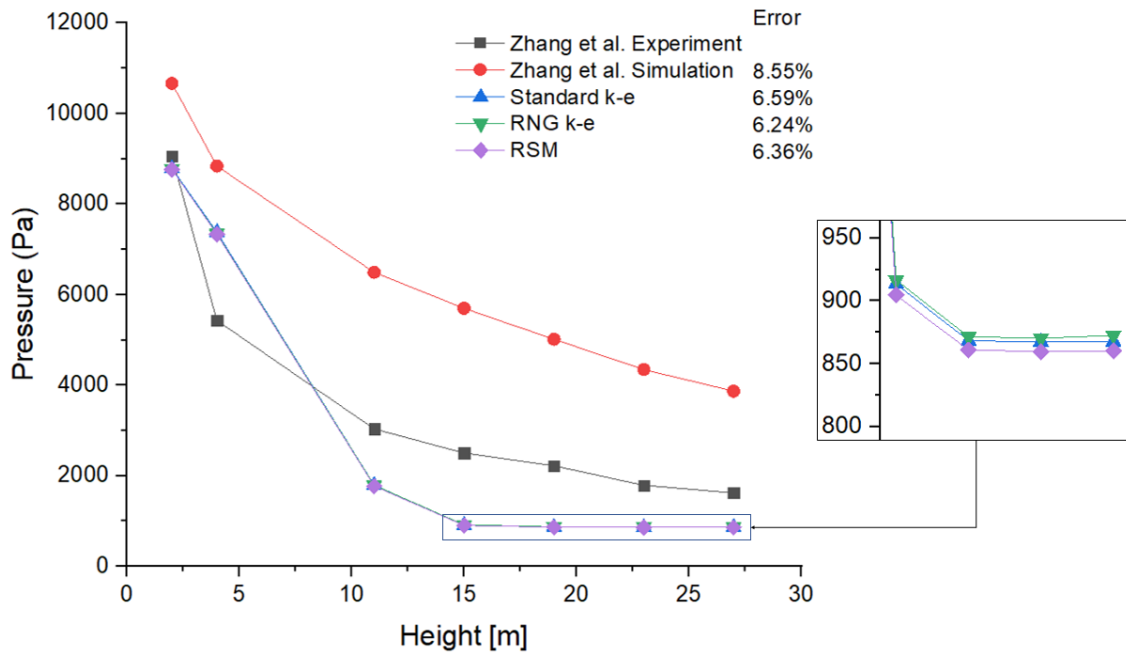
Fig. 5. Pressure comparison graph between simulation results and Zhang *et al.,* research
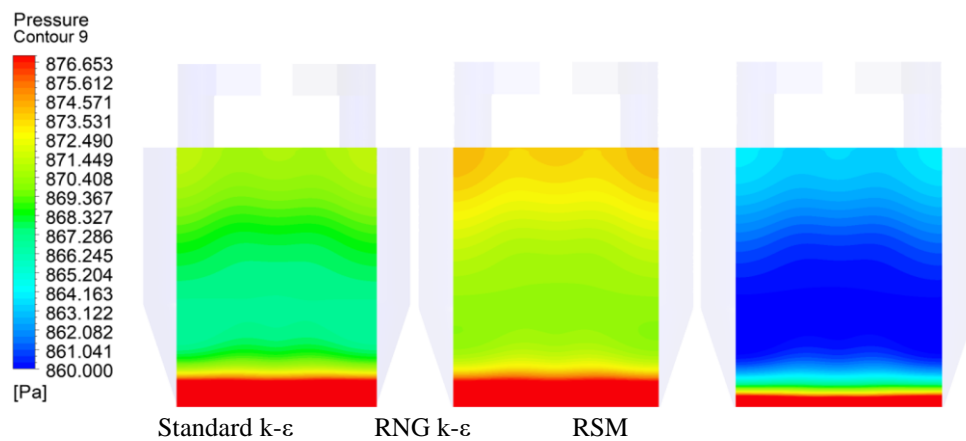
Fig. 6. Comparison of pressure inside the furnace with 3 turbulence models

To ensure that the simulation results have reached a stable state, it is necessary to check the mass imbalance value. With the entering mass flow rate of 170.16 kg/s and the exiting mass flow rate of 170.155 kg/s, there is a 0.003% mass imbalance, ilustrated in Table 6. The maximum percentage of mass imbalance allowed is 0.5% of the incoming mass flow rate [26].

Table 6
Mass imbalance

Name	Mass Flow Rate (kg/s)
Inlet	170.16
Outlet	170.155
Mass Imbalance	0.003 %

3.2 Hydrodynamic Analysis
3.2.1 Solid volume fraction distribution

From Figure 7, it can be observed that from the 10th second to the 40th second, the solid volume fraction expands to a height of 15 m with a value around 0.05 to 0.1 because it is driven by air entering the furnace. This will affect the pressure distribution in the area. The solid pressure equation explains the relationship between solid volume fraction and pressure for granular flow [22].

$$p_s = \alpha_s \rho_s \Theta_s + 2\rho_s(1 + e_{ss})a_s{}^2 g_{0,ss}\Theta_s \qquad (8)$$

The solid pressure symbolized by p_s, is a pressure generated by the distribution of solid particles. The volume fraction of a solid symbolized by α_s became one of the factors that can affect the pressure value, as stated by Feng *et al.,* [30].
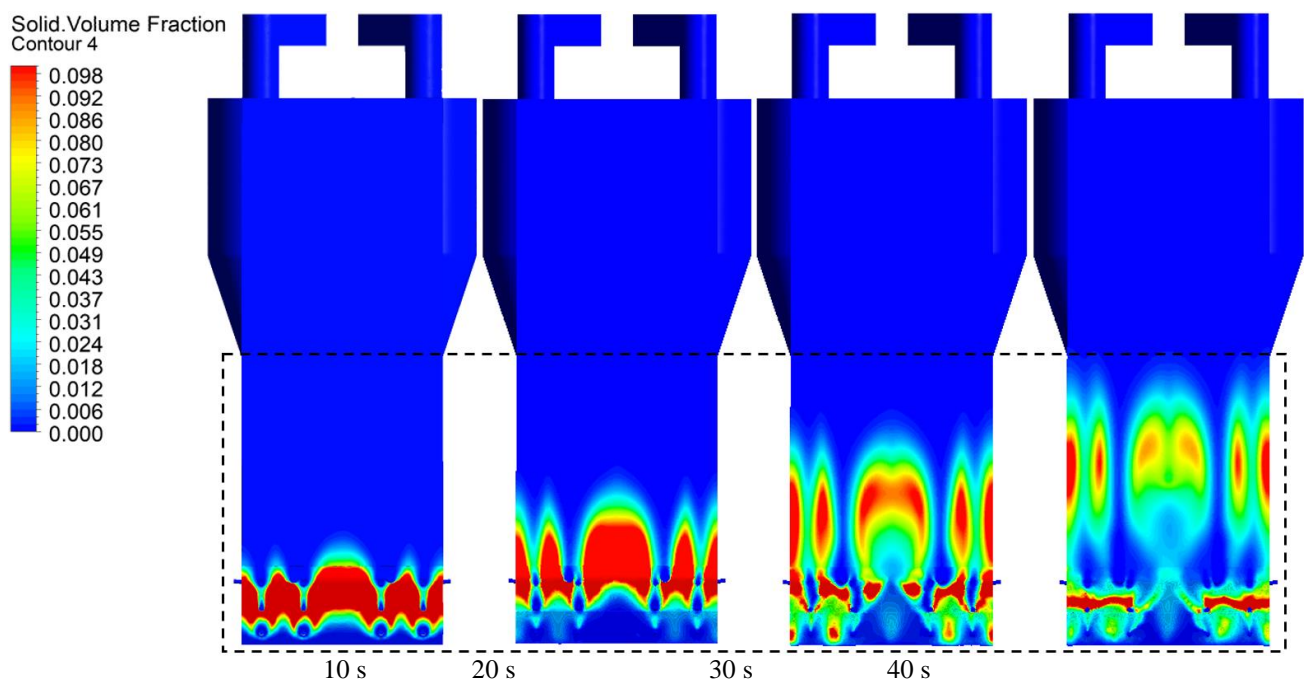
Fig. 7. Solid volume fraction distribution at 4 time intervals

3.2.2 Pressure distribution

Figure 8 conveys that from the 10th second to the 40th second, the area of high pressure expands to a height of 15 m from the furnace's bottom with a value of 3 kPa to 10 kPa. This is caused by the solid volume fractions distribution in the area.
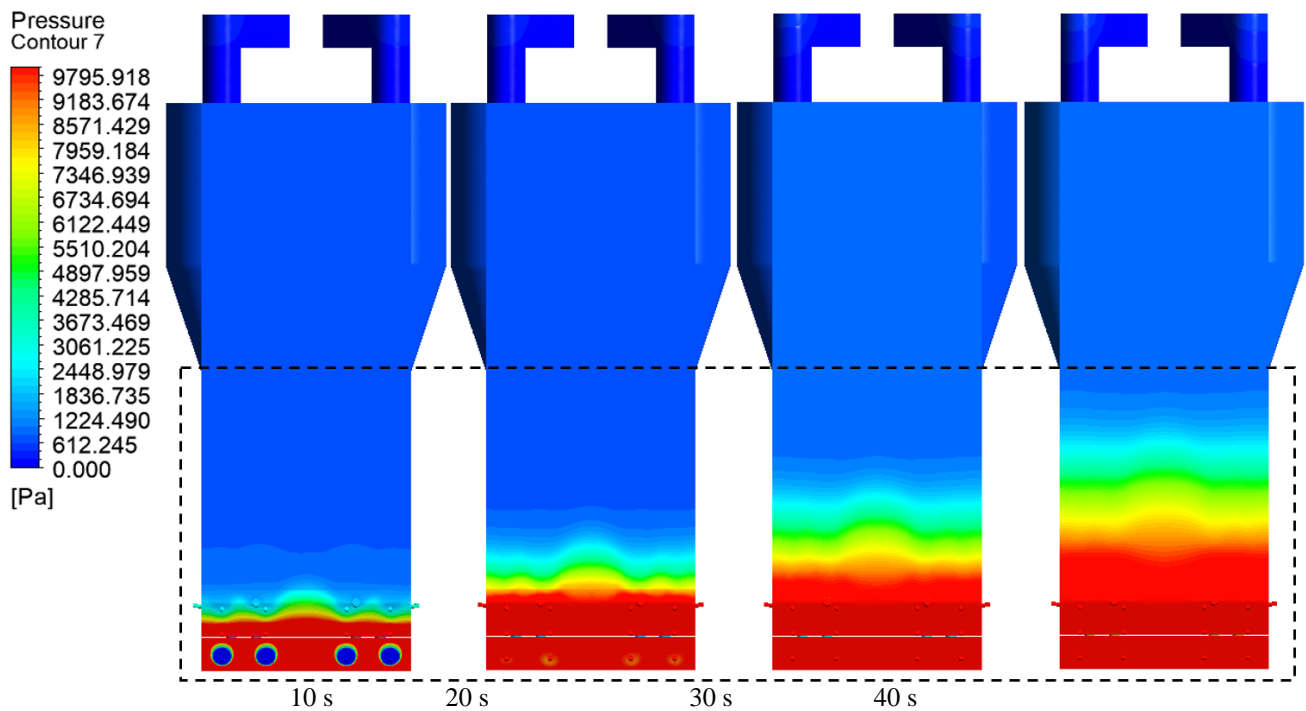
Fig. 8. Pressure distribution at 4 time intervals

The lowest pressure value is located at the outlet line. Figure 9 shows that the pressure in the area is much lower than the pressure in the cyclone because the air that enters the outlet channel directly exits through the outlet. The pressure at the outlet line is around 0.1 kPa, while the pressure in the cyclone is around 0.9 kPa. This will affect the velocity distribution on the outlet line.
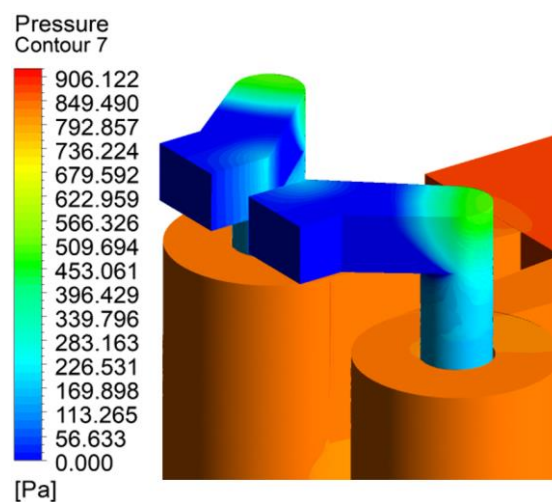
Fig. 9. Pressure distribution on outlet channels and cyclones

The flows from the area with higher pressure to the area with lower pressure. This is based on Bernoulli's law which is stated in the Eq. (9) [31].

$$\frac{dP}{\rho} + \frac{1}{2}d(V^2) + gdz = 0 \tag{9}$$

This remarks that lower pressure in an area creates a higher incoming velocity. This is also stated in research by Guo *et al.,* [32].

3.2.3 Velocity distribution

The air velocity vector in the CFB boiler from the 10th second to the 40th second is shown in Figure 10. The air velocity at the outlet channel is higher than in other areas, with a value between 30 m/s to 50 m/s. This is due to pressure on high cyclones and pressure on a low outlet so that the fluid flows from the cyclone to the outlet channel at high velocity.
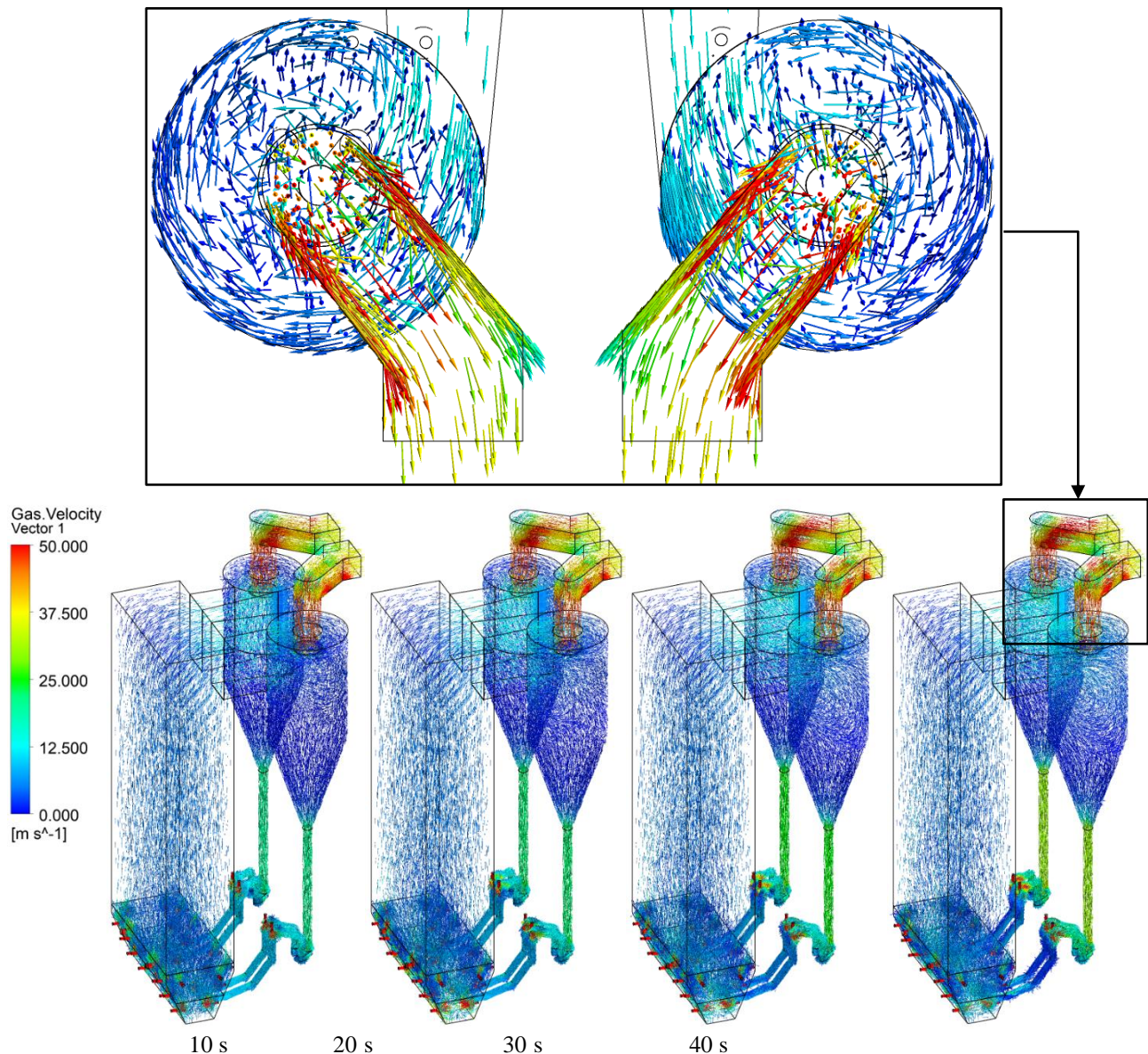
Fig. 10. Velocity distribution at 4 time intervals

The air velocity at the outlet channel rises with time changes. The velocity has increased from 43 m/s to 50 m/s. This velocity distribution is shown in Figure 11. When air enters the furnace, it collides with a pile of solid particles, which reduce the air's velocity. After the solid particles are dispersed, the air velocity increases to a steady state.

145
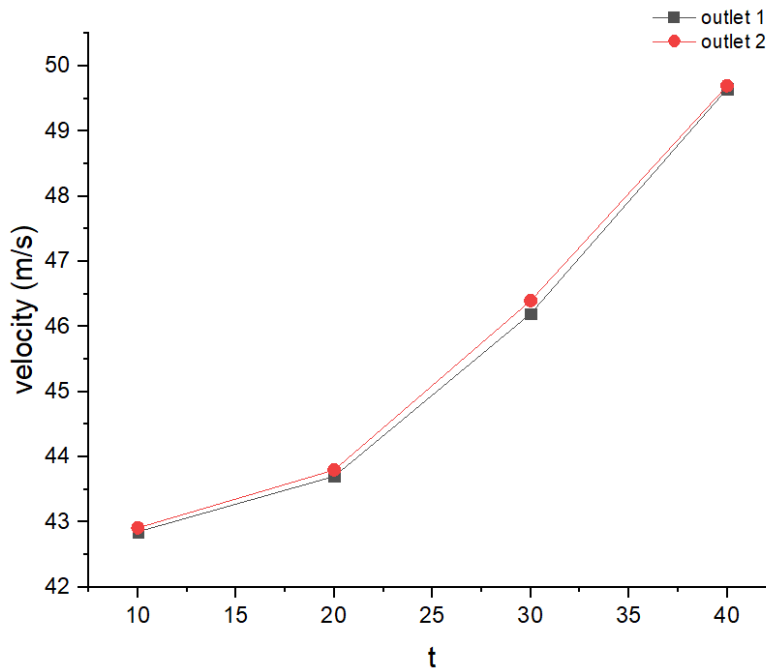
Fig. 11. Velocity graph on outlet channels

As the velocity of the outlet channel increases over time, according to Kaya *et al.,* this will affect the distribution of wall shear stress in the area. The relationship can be seen in Eq. (10) [31,33].

$$\tau_W = \mu \frac{u}{y} = \rho v \frac{u}{y} \qquad (10)$$

The velocity is directly proportional to the wall shear stress. This means that the wall shear stress will also be high if the air velocity is high.

3.2.4 Distribution of wall shear stress

In the CFB boiler from the 10th second to the 40th second, the distribution of wall shear stress is ilustrated in Figure 12. On the outlet wall, the wall shear stress increases. The value of the increase is shown by the graph in Figure 13, which is from 0.75 Pa to 1.1 Pa. This is due to the growth of air velocity outlet channel that makes the change in wall shear stress directly proportional to the change in velocity.
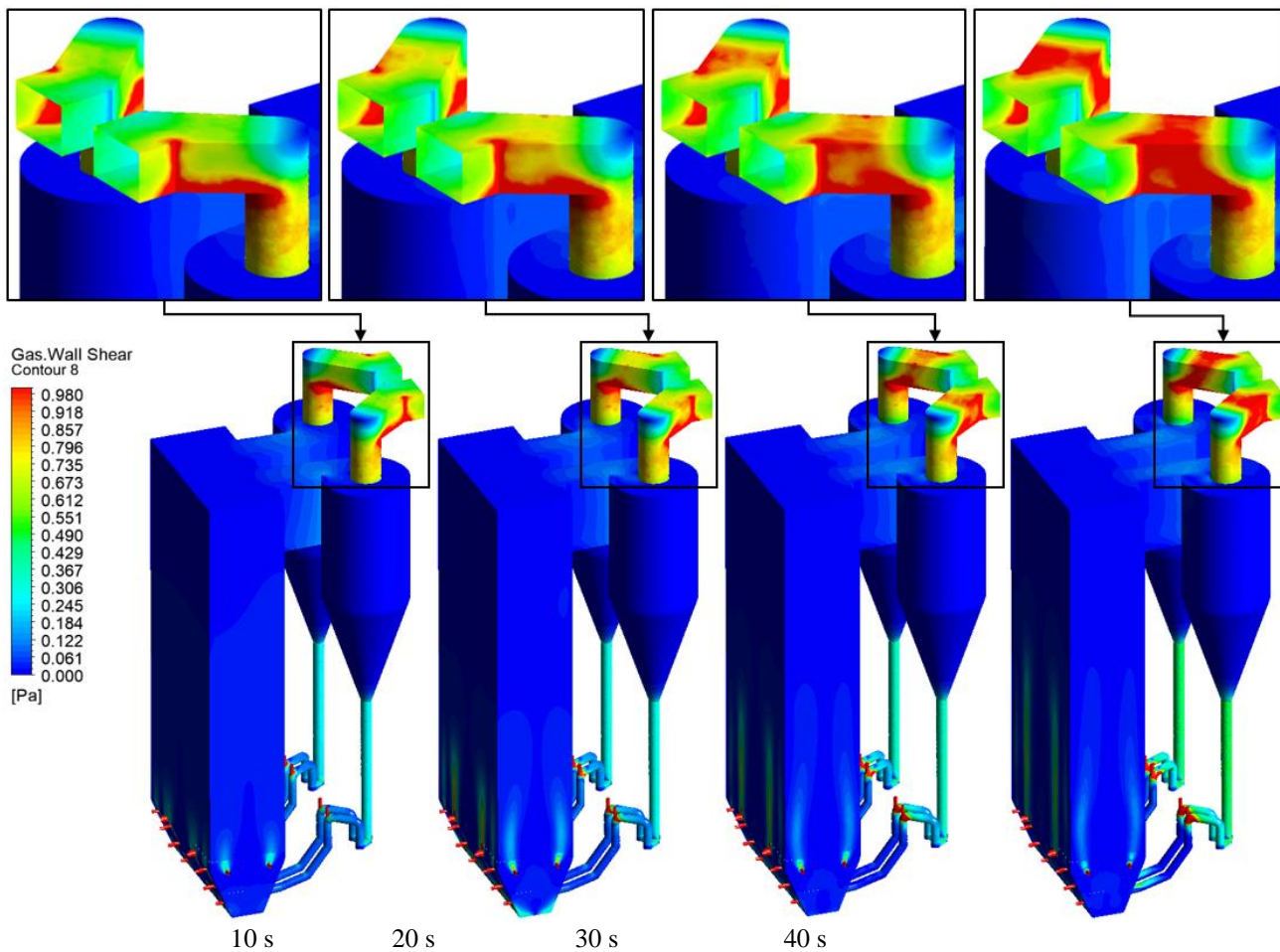
Fig. 12. Wall shear stress distribution at four time intervals
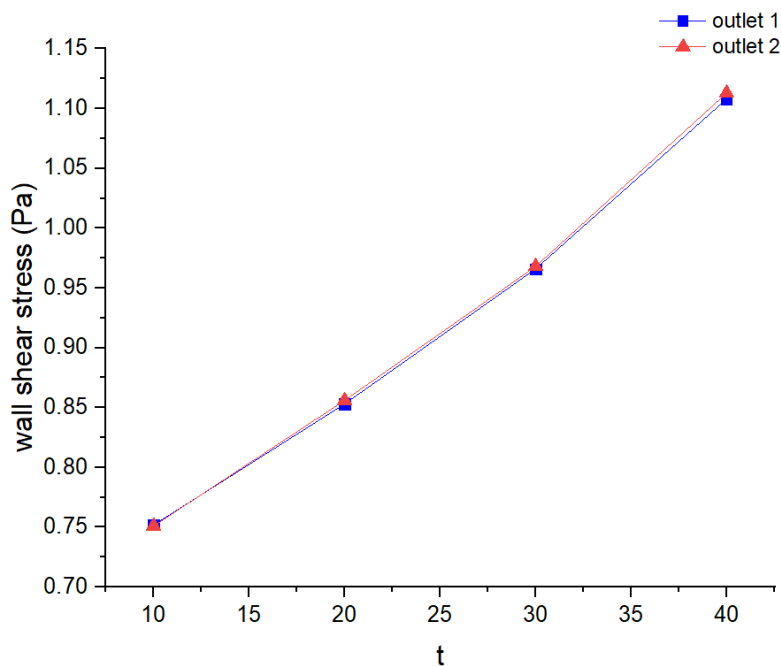
Fig. 13. Wall shear stress graph on both outlet channel walls

4. Conclusions

From the testing of three turbulence models in the CFB boiler simulation, the error value of the experimental data obtained is 6.59% using standard $k - \varepsilon$ models, 6.36% using RSM, and the smallest number is 6.24% using the RNG $k - \varepsilon$ model. As a consequence, since the RNG $k - \varepsilon$ model results are the closest to the experimental data, it can be said that it is the most appropriate turbulence model for the CFB boiler simulation.

From the 10th second to the 40th second, the solid volume fraction in the CFB boiler extends further to a height of 15 m from the furnace's bottom. The solid volume fraction range is from 0.05 to 0.1.

The pressure in the CFB boiler changes from the 10th second to the 40th second, where high pressure expands at the bottom of the furnace to a height of 15 m. Pressure mark in the area ranges from 3 kPa to 10 kPa.

The velocity of the CFB boiler changes from the 10th second to the 40th second when the velocity at the outlet line increases. Velocity values in the area increased from 43 m/s to 50 m/s.

On the outlet channel of CFB boiler, the wall shear stress increases from 10th second to 40th second. The wall shear stress in the area increased from 0.75 Pa to 1.1 Pa.

References

[1] Yacob, Noraishah Shafiqah, and Hassan Mohamed. "Investigating the Palm Oil Mill Wastes Properties for Thermal Power Plants." *Journal of Advanced Research in Fluid Mechanics and Thermal Sciences* 88, no. 2 (2021): 1-13. https://doi.org/10.37934/arfmts.88.2.113

[2] Yacob, Noraishah Shafiqah, and Hassan Mohamed. "Investigation of palm oil wastes characteristics for co-firing with coal." *Journal of Advanced Research in Applied Sciences and Engineering Technology* 23, no. 1 (2021): 34-42. https://doi.org/10.37934/araset.23.1.3442

[3] Government of Indonesia (GOI). "Indonesia long-term strategy for low carbon and climate resilience 2050." *Indonesia LTS-LCCR 2050* (2021).

[4] Zakaria, Sazalina, Radin Diana R. Ahmad, Ahmad Rosly Abbas, and Mohd Faizal Mohideen Batcha. "Greenhouse Gas Emission Intensity Assessment for Power Plants in Peninsular Malaysia." *Journal of Advanced Research in Fluid Mechanics and Thermal Sciences* 88, no. 2 (2021): 14-26. https://doi.org/10.37934/arfmts.88.2.1426

[5] Noor, Noor Akma Watie Mohd, Hasril Hasini, Muhamad Shazarizul Haziq Mohd Samsuri, and Meor Mohd Faisal Meor Zulkifli. "CFD Analysis on the Effects of Different Coal on Combustion Characteristics in Coal-fired Boiler." *CFD Letters* 12, no. 10 (2020): 128-138. https://doi.org/10.37934/cfdl.12.10.128138

[6] Xiao, Yuan, Guoliang Song, Zhao Yang, Xueting Yang, Chao Wang, Zengcai Ji, Qinggang Lyu, and Xingshun Zhang. "Application of post-combustion ultra-low NOx emissions technology on coal slime solid waste circulating fluidized bed boilers." *Waste Management* 137 (2022): 72-80. https://doi.org/10.1016/j.wasman.2021.10.035

[7] Leckner, Bo, and Alberto Gómez-Barea. "Change of existing circulating fluidized bed boilers to oxy-firing conditions for CO2 capture." *Applications in Energy and Combustion Science* 8 (2021): 100042. https://doi.org/10.1016/j.jaecs.2021.100042

[8] Ludowski, Paweł, Dawid Taler, and Jan Taler. "Identification of thermal boundary conditions in heat exchangers of fluidized bed boilers." *Applied thermal engineering* 58, no. 1-2 (2013): 194-204. https://doi.org/10.1016/j.applthermaleng.2013.03.064

[9] Zhu, Qian. "Developments in circulating fluidised bed combustion." *IEA Clean Coal Centre* (2013).

[10] Gu, Jinrao, Qinwen Liu, Wenqi Zhong, and Aibing Yu. "Study on scale-up characteristics of oxy-fuel combustion in circulating fluidized bed boiler by 3D CFD simulation." *Advanced Powder Technology* 31, no. 5 (2020): 2136-2151. https://doi.org/10.1016/j.apt.2020.03.007

[11]   Wang, Tianyu, Tianqi Tang, Yurong He, and Hongliang Yi. "Analysis of particle behaviors using a region-dependent method in a jetting fluidized bed." *Chemical Engineering Journal* 283 (2016): 127-140. https://doi.org/10.1016/j.partic.2013.10.007

[12]   Fan, Yuesheng, and Pengfei Si. "The Study of Numerical Simulation of Oxygenenriched Burner System." *CFD Letters* 2, no. 4 (2010): 197-207.

[13]   Ji, Jieqiang, and Leming Cheng. "CFD modeling of sodium transformation during high-alkali coal combustion in a large-scale circulating fluidized bed boiler." *Fuel* 279 (2020): 118447. https://doi.org/10.1016/j.fuel.2020.118447

[14]   Wu, Ying, Daoyin Liu, Lunbo Duan, Jiliang Ma, Jie Xiong, and Xiaoping Chen. "Three-dimensional CFD simulation of oxy-fuel combustion in a circulating fluidized bed with warm flue gas recycle." *Fuel* 216 (2018): 596-611. https://doi.org/10.1016/j.fuel.2017.12.042

[15]   Versteeg, H. K., and W. Malalasekera. "An Introduction to Computational Fluid Dynamics." (2007).

[16]   Kamal, Muhammad Nabil Farhan, Izuan Amin Ishak, Nofrizalidris Darlis, Daniel Syafiq Baharol Maji, Safra Liyana Sukiman, Razlin Abd Rashid, and Muhamad Asri Azizul. "A review of aerodynamics influence on various car model geometry through CFD techniques." *Journal of Advanced Research in Fluid Mechanics and Thermal Sciences* 88, no. 1 (2021): 109-125. https://doi.org/10.37934/arfmts.88.1.109125

[17]   Xu, Linjie, Leming Cheng, Jieqiang Ji, Qinhui Wang, and Mengxiang Fang. "A comprehensive CFD combustion model for supercritical CFB boilers." *Particuology* 43 (2019): 29-37. https://doi.org/10.1016/j.partic.2017.11.012

[18]   Bahnasy, Amal, and A. M. Abdel-Wahab. "Mathematical Model Represents the Effect of Flexible Endoscopy on Suspension Fluid Flow." *Journal of Advanced Research in Fluid Mechanics and Thermal Sciences* 89, no. 1 (2022): 42-61. https://doi.org/10.37934/arfmts.89.1.4261

[19]   Huttunen, Marko, Juho Peltola, Sirpa Kallio, Lassi Karvonen, Timo Niemi, and Ville Ylä-Outinen. "Analysis of the processes in fluidized bed boiler furnaces during load changes." *Energy Procedia* 120 (2017): 580-587. https://doi.org/10.1016/j.egypro.2017.07.175

[20]   Sirisomboon, Kasama, and Porametr Arromdee. "A computational fluid dynamics study of gas–solid distribution of Geldart Group B particles in a swirling fluidized bed." *Powder Technology* 393 (2021): 734-750. https://doi.org/10.1016/j.powtec.2021.08.020

[21]   Amoo, Leye M. "Computational fluid dynamics simulation of Lafia–Obi bituminous coal in a fluidized-bed chamber for air-and oxy-fuel combustion technologies." *Fuel* 140 (2015): 178-191. https://doi.org/10.1016/j.fuel.2014.09.076

[22]   Fluent, A. N. S. Y. S. "ANSYS Fluent Theory Guide; ANSYS." *Inc., Release* 15 (2013).

[23]   Qing, Nelvin Kaw Chee, Nor Afzanizam Samiran, and Razlin Abd Rashid. "CFD Simulation analysis of Sub-Component in Municipal Solid Waste Gasification using Plasma Downdraft Technique." *CFD Letters* 14, no. 8 (2022): 63-70. https://doi.org/10.37934/cfdl.14.8.6370

[24]   Zhang, Nan, Bona Lu, Wei Wang, and Jinghai Li. "3D CFD simulation of hydrodynamics of a 150 MWe circulating fluidized bed boiler." *Chemical Engineering Journal* 162, no. 2 (2010): 821-828. https://doi.org/10.1016/j.cej.2010.06.033

[25]   Rasul, Mohammad. "Thermal Power Plants-Advanced Applications." (2013). https://doi.org/10.5772/46240

[26]   Guide, A. F. T. "Ansys fluent tutorial guide." *Ansys INC nd* 15 (2013).

[27]   Ansys, I. "ANSYS meshing user's guide." *vol* 15317 (2013): 724-746.

[28]   Wanchan, Waritnan, Parinya Khongprom, and Sunun Limtrakul. "Study of wall-to-bed heat transfer in circulating fluidized bed riser based on CFD simulation." *Chemical Engineering Research and Design* 156 (2020): 442-455. https://doi.org/10.1016/j.cherd.2020.02.021

[29]   Hegde, Pranav, SM Abdul Khader, Raghuvir Pai, Masaaki Tamagawa, Ravindra Prabhu, Nitesh Kumar, and Kamarul Arifin Ahmad. "CFD Analysis on Effect of Angulation in A Healthy Abdominal Aorta-Renal Artery Junction." *Journal of Advanced Research in Fluid Mechanics and Thermal Sciences* 88, no. 1 (2021): 149-165. https://doi.org/10.37934/arfmts.88.1.149165

[30]   Feng, Xuan, Laihong Shen, and Lulu Wang. "Effect of baffle on hydrodynamics in the air reactor of dual circulating fluidized bed for chemical looping process." *Powder Technology* 340 (2018): 88-98. https://doi.org/10.1016/j.powtec.2018.09.012

[31]   Cimbala, John M., and Yunus A. Cengel. *Fluid mechanics: fundamentals and applications*. McGraw-Hill Higher Education, 2006.

[32]   Guo, Tingting, Zhiqun Daniel Deng, Xiuyan Liu, Dalei Song, and Hua Yang. "Development of a new hull adsorptive underwater climbing robot using the Bernoulli negative pressure effect." *Ocean Engineering* 243 (2022): 110306. https://doi.org/10.1016/j.oceaneng.2021.110306

[33]   J Kaya, Recep, Gokhan Deveci, Turker Turken, Reyhan Sengur, Serkan Guclu, Derya Y. Koseoglu-Imer, and Ismail Koyuncu. "Analysis of wall shear stress on the outside-in type hollow fiber membrane modules by CFD simulation." *Desalination* 351 (2014): 109-119. https://doi.org/10.1016/j.desal.2014.07.033